Advanced Lithium-Ion Batteries for Plug-in Hybrid-Electric Vehicles

Paul Nelson
Argonne National Laboratory, 9700 S. Cass Ave, Argonne, IL 60439
630-252-4503, Fax 630-252-4176

Khalil Amine, Aymeric Rousseau, Argonne National Laboratory
Hiroyuki Yomoto, EnerDel Corp.

Abstract

In this study, electric-drive vehicles with series powertrains were configured to utilize a lithium-ion battery with very high power and achieve sport-sedan performance and excellent fuel economy. The battery electrode materials are $LiMn_2O_4$ and $Li_4Ti_5O_{12}$, which provide a cell area-specific impedance of about 40% of that of the commonly available lithium-ion batteries. Data provided by EnerDel Corp. for this system demonstrate this low impedance and also a long cycle life at 55°C. All the batteries for these vehicles were designed to deliver 100 kW of power at 90% open-circuit voltage to provide high battery efficiency (97–98%) during vehicle operation. This heats the battery by only 1.8°C per hour of travel on the urban dynamometer driving schedule (UDDS) cycle, which essentially eliminates the need for battery cooling. Three vehicles were designed, each with series powertrains and simulation test weights between 1,575 and 1,633 kg: a hybrid electric vehicle (HEV) with a 45-kg battery, a plug-in HEV (PHEV)10 with a 60-kg battery, and a PHEV20 with a 100-kg battery. Vehicle simulation tests on Argonne National Laboratory's simulation software, the Powertrain System Analysis Toolkit (PSAT), which was developed with MATLAB/Simulink, showed that these vehicles could accelerate to 60 miles per hour in 6.2 to 6.3 seconds and achieve fuel economies of 50 to 54 miles per gallon on the UDDS and highway fuel economy test (HWFET) cycles. This type of vehicle shows promise of having a moderate cost if it is mass produced because there is no transmission, the engine and generator may be less expensive since they are designed to operate at only one speed, and the battery electrode materials are inexpensive.

Keywords: vehicle simulation, lithium-ion batteries, series-engine hybrid

1. Introduction

Lithium-ion batteries show promise for powering hybrid electric vehicles (HEVs) and plug-in hybrid vehicles (PHEVs), but the batteries under development differ widely in their capabilities. Also, a variety of vehicle types are under consideration, and the requirements for their batteries vary considerably; some demand high energy per unit volume and weight, and others place greater emphasis on high power. For these vehicle applications, the batteries are required to have safe and consistent performance throughout a life of about 15 years and be available in mass production at a moderate price.

2. Status of Advanced Battery Development

Table 1 presents the characteristics of several lithium-ion batteries in various stages of development. These batteries promise markedly different levels of performance for the various criteria for which batteries are evaluated for the HEV and PHEV applications.

The $LiNi_{0.8}Co_{0.15}Al_{0.05}O_2$ (NCA)-graphite system has good power and energy characteristics because of its high voltage, good electrode-specific capacities, and good area-specific impedance (ASI) [1, 2]. Projections show it would have a moderate cost in production and good life if the state of charge (SOC) is maintained between 90% and 30%. Work remains to be done to increase the useful fraction of the SOC range and achieve excellent battery life (15 years). Also, at present, the NCA electrode has a tendency to release significant amounts of oxygen during thermal runaway, resulting in oxidation of the electrolyte. The graphite electrode adds chemically bound energy to such a catastrophic incident.

The $LiFePO_4$ (LFP) electrode is more stable and does not generate oxygen during heating; thus, it appears to be safer at this time than the NCA electrode [3, 4]. Otherwise, the performances of the first two systems in Table 1 are expected to be similar, but the LFP-graphite system shows promise of a slightly lower raw material cost. However, developing a low-cost process for preparing nano-$LiFePO_4$ material requires additional effort.

Table 1: Selected Lithium-Ion Battery Systems for Plug-in Hybrid Electric Vehicles

System	NCA-Graphite	LFP-Graphite	MS-TiO	MNS-TiO	MN-Graphite
Electrodes Positive Negative	$LiNi_{0.8}Co_{0.15}Al_{0.05}$ Graphite	$LiFePO_4$ Graphite	$LiMn_2O_4$ $Li_4Ti_5O_{12}$	$LiMn_{1.5}Ni_{0.5}O_4$ $Li_4Ti_5O_{12}$	$Li_{1.2}Mn_{0.6}Ni_{0.2}O_2$ Graphite
Capacity, mAh/g Positive Negative	 155 290	 162 290	 100 170	 130 170	 275 290
Voltage, 50% SOC	3.6	3.35	2.52	3.14	3.9
ASI for 10-s Pulse, ohm-cm^2	25	25	9.2	100	25
Safety	Fair	Good	Excellent	Excellent	Excellent
Life Potential	Good	Good	Excellent	Unknown	Unknown
Cost	Moderate	Moderate	Low	Moderate	Moderate
Status	Pilot Scale	Pilot Scale	Develop.	Research	Research

The third system in Table 1, MS-TiO, has electrodes with low capacity, and the couple has lower voltage than those of the first two systems. The lithium-spinel positive electrode does not form a good couple with a graphite negative electrode because manganese dissolves in the electrolyte and poisons the graphite electrode [5–8]. Against a lithium-titanate electrode, however, it forms a very stable couple, albeit with a low voltage. The titanate electrode has a voltage that is 1.5 V higher than that of lithium, whereas a good graphite electrode is only about 0.1 V higher. The combination of low voltage and low specific capacities for both electrodes in the MS-TiO system results in lower specific energy for the battery than for most lithium-ion systems. This is

somewhat mitigated by the very stable performance and long cycle life for 100% discharges, as discussed below, which permit operating MS-TiO batteries over the SOC range of 100% to 10% for the PHEV application. Another favorable characteristic of the MS-TiO system is very low ASI, which results in very high power. The safety characteristics appear to be excellent; it is very tolerant of excessive voltage upon charging, with a very reduced likelihood of lithium deposition, and the stored chemical energy in the system is very low when compared with that of systems with graphite electrodes. As shown by the data that follow, the cycle life for the MS-TiO system is excellent. Cost projections are only tentative, but the MS-TiO system appears to have inherent advantages over the other systems in that its electrode materials are low in cost and plentiful.

The fourth system in Table 1, MNS-TiO, is similar to the MS-TiO system, but with a manganese-nickel spinel positive electrode that operates at a very high voltage versus lithium (4.8 V at full charge) and with improved capacity relative to manganese spinel. At present, the ASI is higher than it is for the MN-TiO system, but it is believed that this can be improved sufficiently to achieve the required power (100 kW for the PHEVs in this study) for a 40-mi-range PHEV.

The highest-capacity positive electrode in Table 1 is in the MN-graphite system developed at Argonne [9, 10]. This would result in the lowest battery weight for a 40-mile PHEV for the batteries reviewed in Table 1. This system requires more development work, but it illustrates the improvements in battery performance that may come in the future.

3. Spinel-Titanate Battery Performance Modeling

3.1 Approach

Despite its low capacity and low voltage, we have studied the MS-TiO system to determine if a battery-vehicle combination could be found that exploits the very high power of the MS-TiO system. A type of vehicle that may be particularly enhanced by very high battery power is one with a series-connected powertrain with sport-sedan performance. For such a vehicle to achieve high fuel economy, the engine should operate close to its peak efficiency, which requires that the battery have high power to accept charging at a high rate. Therefore, we decided to design a battery that could discharge at the 100-kW rate for a 10-s burst at 90% open-circuit voltage (OCV) so that the overall battery efficiency would exceed 97% for most vehicle-driving cycles. The high battery power would also make possible higher vehicle performance than is usually expected of HEVs — more like that of a sport-sedan.

Through a collaboration between Argonne and EnerDel, experimental data became available to establish the low ASI of the MS-TiO system and the promising long cycle life for deep discharges, which justify the assumption that the battery can be operated between 100% and 10% SOC. Two types of modeling were required to characterize the battery for vehicle simulation studies:
(1) design modeling to determine the battery weight, volume, and electrical performance and
(2) impedance modeling. The experimental data and modeling are discussed below.

3.2 Experimental Data

Tests with a 1.8-Ah MS-TiO cell demonstrated outstanding power; 97% of the capacity measured at the 1C discharge rate was delivered at the 50C rate (Fig. 1) [11]. These results were correlated to obtain the impedance equations required for the vehicle simulation tests.

The capacity stability was demonstrated in tests in which the entire cell capacity was discharged and charged at the 5C rate at an elevated temperature of 55^{o}C, to accelerate degradation, for 2,300 cycles with little indication of capacity loss (Fig. 2) [11]. Pulse power characterization tests were carried out at 30^{o}C after 1,000 and 2,000 cycles and demonstrated little loss of power with

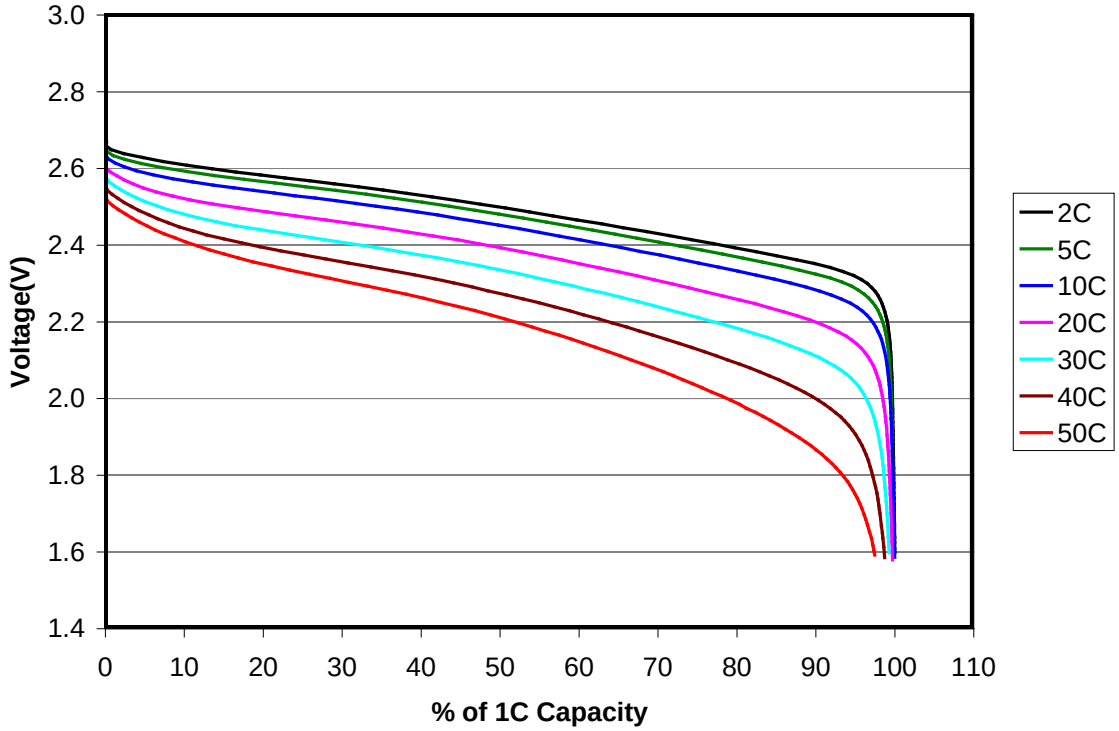

Figure 1: Lithium-Manganese Spinel/Lithium-Titanate 1.8-Ah Cell Charged at 1C Rate and Discharged at Varying Rates at 30°C [11]

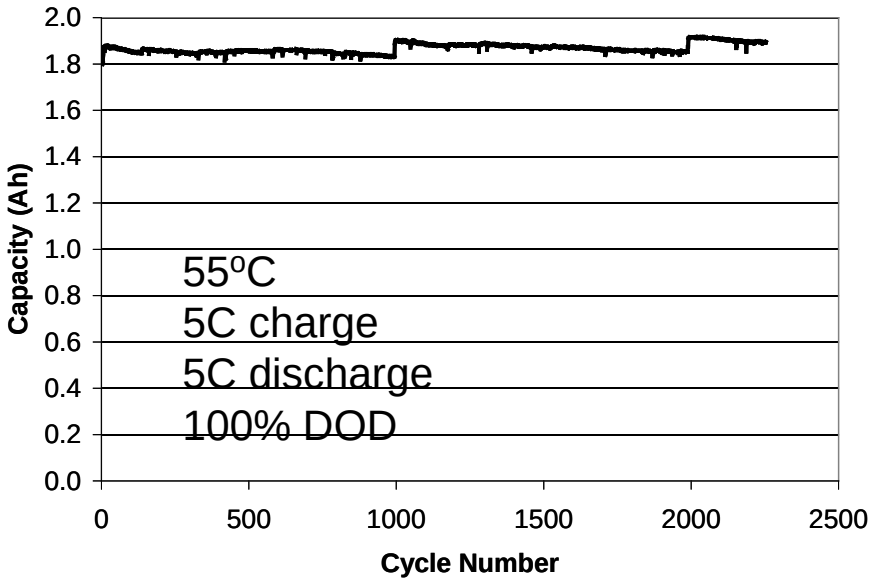

Figure 2: Deep Discharging of Lithium-Manganese Spinel/ Lithium-Titanate Cell to Demonstrate Long Cycle Life [11]

cycling. The promising results obtained in these aggressive tests at high temperature indicate that MS-TiO batteries may meet achieve the 5,000 cycles required for the PHEV application.

3.3 Battery Design Modeling

We have developed a method, based on Excel spreadsheets, for designing cells and batteries that has been applied to several battery systems. In recent years, the method has been used primarily for designing lithium-ion batteries for HEVs and PHEVs [12, 13]. One form of input for this method is test results from measurements of capacity and ASI on small cells with areas of only a few square centimeters. It is also possible to accept data from larger cells by accounting for the resistance of the current collection system in the tested cell. The method calculates the volumes and weights of all of the cell and battery components and the electrical performance of the battery. By this method, three batteries were designed for a series-connected vehicle from the data in Table 1 for the MS-TiO system and from other proprietary input. The results are shown in Tables 2 and 3. **No callout for Reference 14**

Table 2. Cell Parameters for Lithium-Manganese Spinel/ Lithium-Titanate Batteries for HEVs and PHEVs

Cell Parameter	HEV	10-Mile* PHEV	20-Mile* PHEV
Cell Capacity (1/C rate), Ah	10.0	16.6	33.3
Positive First Charge Loading Density, mAh/cm^2	0.54	0.88	1.79
Negative-to-Positive 1st Charge Capacity Ratio	1.0	1.0	1.0
Maximum Voltage on Charging, V	2.7	2.7	2.7
Average Voltage on Discharge, V	2.51	2.51	2.51
Positive Electrode			
Active Material	$Li_{1.06}Mn_{1.94}O_4$	$Li_{1.06}Mn_{1.94}O_4$	$Li_{1.06}Mn_{1.94}O_4$
Thickness of Coating (each side), µm	25	40	82
Negative Electrode Material			
Active material	$Li_4Ti_5O_{12}$	$Li_4Ti_5O_{12}$	$Li_4Ti_5O_{12}$
Thickness of Coating (each side), µm	21	34	70
Total Cell Area, cm^2	20,500	20,500	20,500
Cell Dimensions, mm			
Height	189	219	219
Width	104	116	187
Thickness	12.2	12.4	12.5
Cell Weight, g	471	648	1102
Power, W	1251	1251	1251
Cell-specific Power, kW/kg	2.66	1.93	1.14
Cell-specific Energy (1/C rate), Wh/kg	53	64	76

*Based upon energy usage of 300 Wh/mi.

Table 3: Battery Parameters for Lithium-Manganese Spinel/
Lithium-Titanate Batteries for HEVs and PHEVs

Battery Parameter	HEV	10-Mile* PHEV	20-Mile* PHEV
Number of Cells in Battery	80	80	80
Number of Modules (10 cells each)	8	8	8
Energy Storage (1-h rate), kWh	2.0	3.3	6.7
Useable Energy			
HEV, 60% to 35% SOC	0.50		
PHEV, 100% to 10% SOC		3.0	6.0
Discharge Power (10 s), kW	100	100	100
Discharge Voltage at Full Power (50% SOC), V	181	181	181
% of Open-circuit Voltage (OCV)	90	90	90
Power Density, kW/L	3.59	2.81	1.81
Current on Discharge, A			
At Rated Power (50% SOC, 90% OCV)	552.5	552.5	552.5
Maximum Allowed (30 s)	560.0	560.0	560.0
Maximum Regeneration Power, kW			
Short-Term (2-s regen braking)	100	100	100
Long-Term (up to 60 s)	70	70	70
Maximum Charge Voltage, V	216	216	216
Insulated Battery Wall Thickness, mm	7	7	8
Battery Dimensions, mm			
Length	852	973	973
Width	266	270	274
Height	123	135	207
Volume, L	28	36	55
Weight, kg	45	60	100
Total Weight of Cells, % of Battery Weight	84	86	88
Cooling Fluid (exterior of modules only)	Air	Air	Air

*Based upon energy usage of approximately 300 Wh/mile.

3.4 Impedance Modeling

On the basis of the data shown in Figures 1 and 2, the impedance of the experimental cell was modeled to fit Equation (1) in Figure 3.

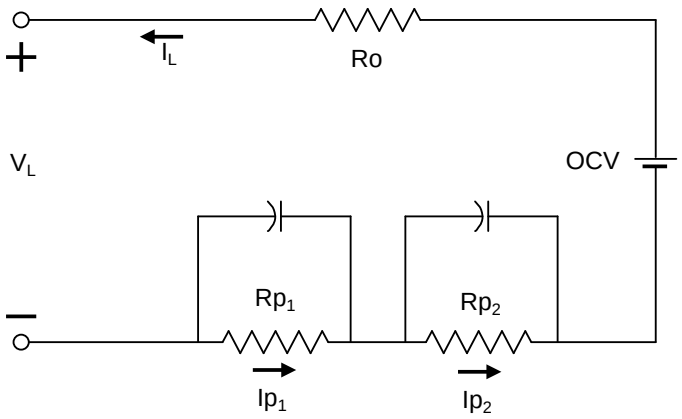

Equation (1) $1000*(OCV-V_L)/I_L = R = Ro+Rp_1*Ip_1/I_L+Rp_2*Ip_2/I_L$

Where,

OCV = open circuit voltage, V
V_L = cell voltage, V
R = total cell impedance, milliohms
Ro = cell internal ohmic resistance, milliohms
Rp_1 = first internal polarization resistance, milliohms
Rp_2 = second internal polarization resistance, milliohms
I_L = cell load current, A
Ip_1 = current through first polarization resistance, A
Ip_2 = current through second polarization resistance, A

The values for Ip_1 and Ip_2 are derived by integration of the differential equation:

Equation (2) $dIp/dt = (I_L-Ip)/\tau$

Figure 3: Impedance Model for Lithium-Manganese Spinel/Lithium-Titanate Batteries [14]

The results were adjusted to simulate a 1-Ah cell to facilitate their use in calculating battery impedance for any desired capacity and number of cells. They are shown in Table 4, in which the values of Tau_1 and Tau_2 are time constants expressed in seconds for the two polarization resistances in the model.

The impedance parameters for the 1-Ah Cell of Table 4 were applied for the 100-kW batteries of Table 3, with the result illustrated in Table 5.

Table 4: Parameters for Calculating Impedance of a 1-Ah Lithium-Manganese Spinel/Lithium-Titanate Cell

Depth of Discharge (DOD), %	OCV	Ro	Rp_1	Rp_2	Tau_1	Tau_2
0	2.661	0.00320	0.00220	0.00100	10	270
10	2.621	0.00320	0.00220	0.00120	10	270
20	2.593	0.00320	0.00209	0.00130	10	270
30	2.569	0.00320	0.00220	0.00130	10	270
40	2.543	0.00320	0.00230	0.00140	10	270
50	2.514	0.00320	0.00266	0.00140	10	270
60	2.483	0.00320	0.00313	0.00132	10	270
70	2.446	0.00320	0.00355	0.00108	10	270
80	2.408	0.00320	0.00420	0.00100	10	270
90	2.368	0.00320	0.00500	0.00100	10	270
95	2.336	0.00380	0.00600	0.00100	10	270
100	1.6	0.00440	0.00700	0.00100	10	270

Table 5: Impedance, Voltage, and Current for 10-Second Power Burst for 100-kW Lithium-Manganese Spinel/Lithium-Titanate Batteries

10-s Burst Discharge at 100 kW					10-s Burst Power at 560 A, kW
SOC, %	R-10s	V	% OCV	A	
100	0.0342	195.4	91.8	511.8	108.5
90	0.0343	191.8	91.5	521.3	106.7
80	0.0338	189.6	91.4	527.3	105.6
70	0.0343	187.2	91.1	534.2	104.3
60	0.0348	184.6	90.7	541.7	103.0
50	0.0364	181.0	90.0	552.5	101.2
40	0.0386	176.8	89.0	565.6	99.1
30	0.0405	172.2	88.0	580.8	96.9
20	0.0435	166.5	86.5	600.4	94.2
10	0.0472	160.0	84.4	625.2	91.3
5	0.0562	149.2	79.9	670.1	87.0
0	0.0652				

4. Vehicle Simulation for High-Power Batteries

4.1 Approach

The Powertrain System Analysis Tool (PSAT) [15, 16], developed with MATLAB/Simulink, is a vehicle-modeling package used to simulate performance and fuel economy. It allows one to realistically estimate the wheel torque needed to achieve a desired speed by sending commands to different components, such as throttle position for the engine, displacement for the clutch, gear number for the transmission, or mechanical braking for the wheels. In this way, we can model a

driver who follows a predefined speed cycle. Moreover, as components in PSAT react to commands realistically, we can employ advanced component models, take into account transient effects (e.g., engine starting, clutch engagement/disengagement, or shifting), and develop realistic control strategies. Finally, by using test data measured at Argonne's Advanced Powertrain Research Facility (APRF), PSAT has been shown to predict the fuel economy of several hybrid vehicles within 5% on the combined cycle. PSAT is the primary vehicle simulation package used to support the U.S. Department of Energy's (DOE's) FreedomCAR research and development activities.

4.2 Vehicle Characteristics

Several vehicles were sized for different specifications on the basis of the same vehicle attributes: HEV, PHEV with a 10-mi all-electric range (AER), and PHEV with a 20 mi AER. The main component masses are shown in Table 6.

Table 6: Mass of Vehicle Components (kg)

Component	HEV	PHEV10	PHEV20
Engine	120	120	120
Generator	86	86	87
Motor	144	144	146
Battery	45	60	100
Vehicle	1575	1590	1633

Table 7 lists the main characteristics of the simulated midsize car.

Table 7: Vehicle Main Specifications

Component	Specifications
Engine	2004 US Prius
Electric machine	Ballard IPT - Induction
Single Gear Ratio	2
Final Drive Ratio	3.8
Frontal Area	2.1 m^2
Drag Coefficient	0.25
Rolling Resist.	0.007 (plus speed-related term)
Wheel radius	0.317 m

As shown in Figure 4, the configuration selected is a series engine hybrid, very similar to the one used in the GM Volt [17].

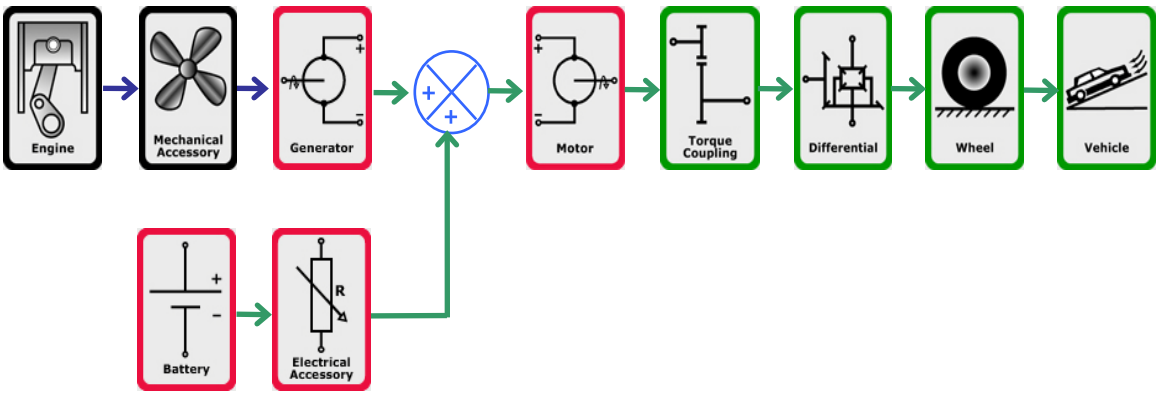

Figure 4: Series Engine Configuration

Five driving cycles are considered in the study to evaluate the impact of advanced lithium ion batteries on fuel economy: UDDS (urban dynamometer driving schedule), HWFET (highway fuel economy test), LA92 (1992 test data from Los Angeles), NEDC (new European driving cycle) and Ford ATDS (Automotive Testing and Development Services). The main characteristics of each cycle are summarized in Table 8.

Table 8: Drive Cycle Characteristics

Characteristic	Unit	UDDS	HWFET	LA92	ATDS	NEDC
Duration	s	1372	764	1435	1799	1180
Distance	km/mi	11.92/7.45	16.38/10.24	15.7/9.81	25.2/15.75	10.9/6.84
Average Speed	mph	19.5	48.26	24.6	31.5	20.86
Average Accel.	m/s2	0.5	0.19	0.67	0.55	0.59
Average Decel.	m/s2	–0.57	–0.22	–0.75	–0.55	–0.78
Number Stops		17	1	16	18	13
Percent Stops		18.92	0.65	16.3	20.73	24.9

Note that all the simulations performed in PSAT represent hot conditions.

4.3 Component Sizing Algorithm

The components of the different vehicles were sized to meet the same vehicle performance values: 0 to 60 mph in less than 7 seconds and gradeability of 6% at 65 mph.

To quickly size the component models of the powertrain, an automated sizing process was developed. A flow chart illustrating the sizing process logic is shown in Fig. 5. While the engine power is the only variable for conventional vehicles, HEVs have two variables: engine power and electric power. In that case, the engine is sized to meet gradeability requirements, while the battery is sized to meet performance requirements. In the study, we also insure that the vehicle can capture the entire energy from regenerative braking during decelerations on the UDDS.

Similar to the HEV configuration, the engine and generator powers are sized to meet gradeability requirements. In addition to HEVs, the battery power has to be sized to follow the UDDS driving cycle while in all-electric mode. Finally, the battery energy is sized to achieve the required AER of the vehicle. The AER is defined as the distance the vehicle can travel on the UDDS without starting the engine. Note that a separate control algorithm is used to simulate the AER. This algorithm forces the engine to remain off throughout the cycle, regardless of the torque request from the driver.

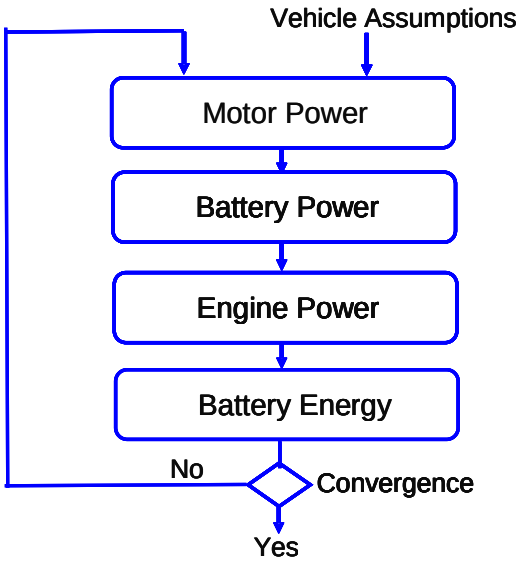

Figure 5: PHEV Component Sizing Process

The main component characteristics resulting from the sizing algorithm are described in Table 9.

Table 9: Component Sizing Results

Parameter	Unit	HEV	PHEV10	PHEV20
Engine Power	kW	100	100	102
Generator Power	kW	95	95	96
Motor Power	kW	130	130	132
Battery Power	kW	100	100	100
Vehicle Mass	kg	1575	1590	1633
Accel. Time 0–60 mph	s	6.2	6.2	6.3

4.4.1 Control Strategy Philosophy

The control strategy of the PHEVs can be separated into two distinct modes, as shown in Fig. 6:

- Charge-depleting (CD) Mode: Vehicle operation on the electric drive, engine subsystem, or both, with a net decrease in battery SOC.

- Charge-sustaining (CS): Vehicle operation on the electric drive, engine subsystem, or both, with a "constant" battery SOC (i.e., within a narrow range), which is similar to that in current production HEVs.

During a simulation, the engine is turned on when the battery SOC is low or the power requested at the wheel cannot be provided by the battery alone. Turning the engine on expends fuel but conserves battery energy, so that more miles can be traveled before the battery reaches its discharged state. When the engine is ON, it is operated close to its best efficiency curve. As a result, the battery is being charged by the engine during low power requests, leading to lower electrical consumption.

The initial SOC of the battery, which is also the battery's maximum charge, is 100%, and the final SOC of the battery, which is also the battery's minimum charge, is 10%. For the CD mode, the engine logic was written in StateFlow and used several conditions, such as battery SOC, motor power limits, and vehicle speed, to determine when the engine should turn on and the output torque of the engine. The logic of the CS mode was similar to that of current HEVs.

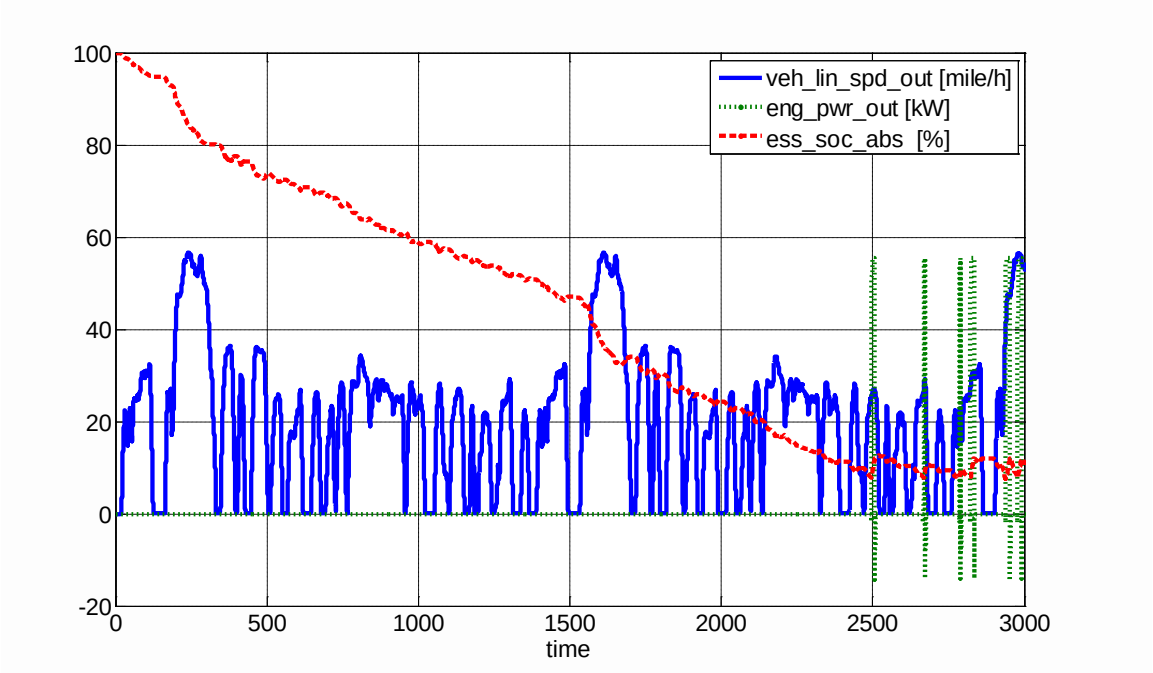

Figure 6: Control Strategy SOC Behavior on the UDDS

4.5 Fuel Economy Results

As previously mentioned, several driving cycles have been considered to evaluate the benefits of the advanced lithium-ion batteries on PHEVs. Table 10 summarizes the electrical consumption on each PHEV vehicle on the first cycle of each drive cycles. These results highlight the differences in aggressiveness in the different drive cycles. As expected, the standardized drive cycles (UDDS, HWFET, and NEDC) require a lower electrical consumption than the cycles that are more "real-world." The ATDS is the most aggressive drive cycle.

Table 10: PHEV Electrical Information

AER	PHEV	UDDS	HWFET	NEDC	LA92	ATDS
10-mi	Elec Cons. First Cycle (Wh/mi)	224.6	204.3	234.1	282.6	190.4(1)
	AER (mi)	13.8	14.3	12.8	10.3	9.5
20 mi	Elec Cons. First Cycle (Wh/mi)	257.9	209.9	241.6	297.9	300.8
	AER (mi)	26.6	28.6	26.5	20.4	19.9

(1) Engine started during the first cycle

Because the primary goal of PHEVs is to maximize fuel displacement, the following analysis focuses on fuel consumption. Figure 7 shows the evolution of the fuel economy when each cycle is repeated 10 times.

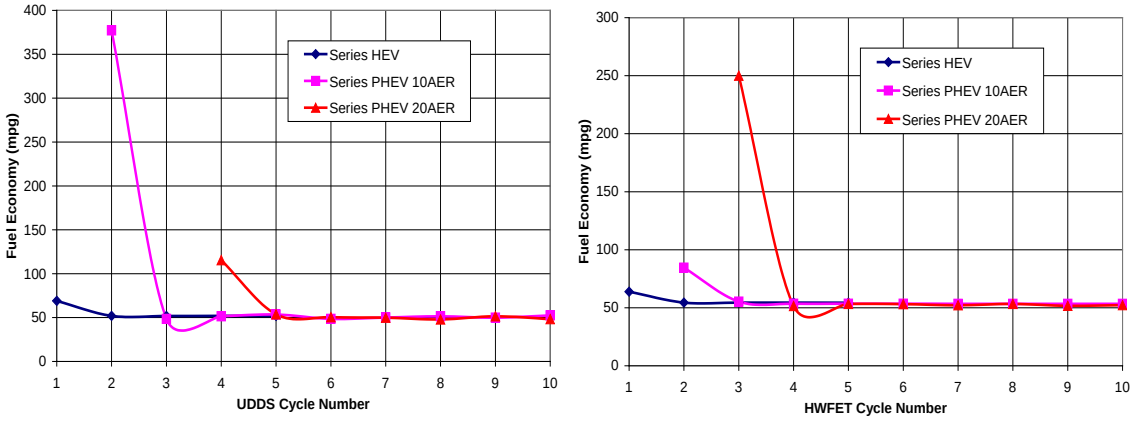

Figure 7: Fuel Economy Evolution on UDDS and HWFET

The benefit of high-power batteries is noticeable in the more aggressive driving cycles (Fig. 8). When an engine start would have been necessary for low-power batteries, the initial distance can be achieved in EV mode without any help from the engine. Note, however, that previous studies [18] have demonstrated the need to know the trip distance to properly minimize fuel consumption. However, higher battery power allows additional flexibility in deciding when to start the engine.

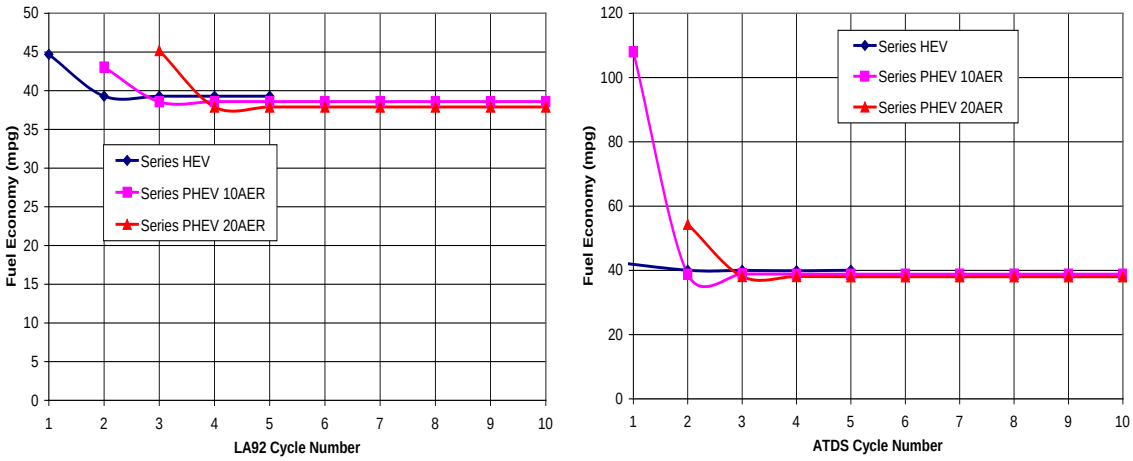

Figure 8: Fuel Economy Evolution on LA92 and ATDS

Table 11 shows the CS fuel economies of the different vehicles. Because of increased vehicle mass, the fuel economy decreases slightly with an increase in AER.

Table 11: CS Fuel Economy (mpg)

Vehicle	UDDS	HWFET	NEDC	LA92	ATDS
HEV	51.9	54.4	52.3	39.3	40.0
PHEV 10	51	53.3	51.5	38.6	38.8
PHEV 20	49.6	52	50.5	37.9	38

Figure 9 shows the evolution of the electrical consumption for the UDDS and ATDS drive cycles. The impact of the cycle aggressiveness can be seen by slope of the electrical consumption. In the case of the ATDS, the slope is much stiffer than for the UDDS.

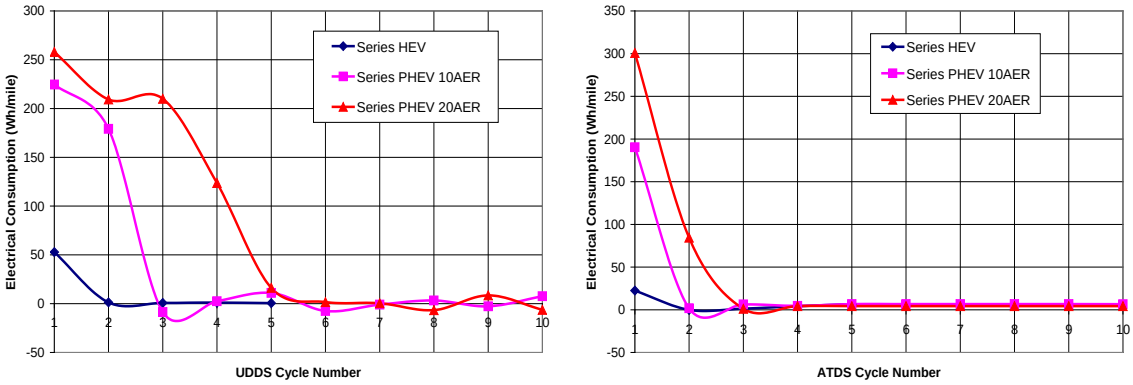

Figure 9: Electrical Consumption Evolution on UDDS and ATDS

The efficiencies of the vehicle components are very high as illustrated in Table 11 for the UDDS cycle. Improvement in the fuel economy for these vehicles could be achieved by increasing the motor efficiency. An additional low-power (30–50 kW) motor could be provided to be used for light loads, when it could operate at a higher efficiency than the high-power motor (130 kW) in the evaluated designs.

Table 11: Component Average Efficiencies on UDDS

Component	HEV	PHEV10	PHEV20
Engine	36.9	37.2	37.2
Generator	91.9	91.9	91.9
Motor	80.4	80.4	80.4
Battery	98.4	97.5	97.4
Gear	97.5	97.5	97.5

The high battery efficiency results in very little battery heating. One hour of travel on the UDDS cycle would heat up the PHEV10 battery by 1.6^{o}C under adiabatic conditions.

5. Conclusions

High vehicle performance, of the type expected from sport-sedans, and high fuel economy can be achieved at the same time by a vehicle having a series powertrain and a high-power manganese spinel/lithium titanate battery. Further improvement in fuel economy might result from improving the motor efficiency. This battery can provide high power at such high battery efficiency that battery cooling is virtually unnecessary. This type of vehicle shows promise of having a moderate cost if it is mass produced because there is no transmission, the engine and generator may be less expensive since they are designed to operate in a narrow range, and the battery electrode materials are inexpensive.

6. Acknowledgments

This work was supported by DOE's FreedomCAR and Vehicle Technology Office under the direction of Tien Duong and David Howell of that program. The submitted manuscript has been created by UChicago Argonne, LLC, Operator of Argonne National Laboratory ("Argonne"). Argonne, a U.S. Department of Energy Office of Science laboratory, is operated under Contract No. DE-AC02-06CH11357. The U.S. Government retains for itself, and others acting on its behalf, a paid-up nonexclusive, irrevocable worldwide license in said article to reproduce, prepare derivative works, distribute copies to the public, and perform publicly and display publicly, by or on behalf of the Government.

7. References

[1] Amine, K., Chen, C.H., Liu, J., Hammond, M., Jansen, A., Dees, D., Bloom, I., Vissers, D., and Henriksen, G., *Journal of Power Sources* 97-8:684–687, 2001.

[2] Abraham, D.P., Liu, J., Chen, C.H., and Amine, K., *Journal of Power Sources* 119:511–516. Sp. Iss. SI, 2003.

[3] Belharouak, I., Lu, W.Q., Vissers, D., et al., *Electrochemistry Communications* 8(2):329–335, 2006.

[4] Doughty, D.H., Roth, E.P., Crafts, C.C., Nagasubramanian, G., Henriksen, G., and Amine, K., *Journal of Power Sources* 146:116–120, 2005.

[5] Amine, K., Liu, J., and Belharouak, I., *Electrochemistry Communications* 7:669–673, 2005.

[6] Amine, K., Liu, J., Belharouak, I., Kang, S.H., Bloom, I., Vissers, D., and Henriksen, G., *Journal of Power Sources* 146:111–115, 2005.

[7] Amine, K., Liu, J., Kang, S., et al., *Journal of Power Sources* 129(1):14–19 , 2004.

[8] Chen, Z., and Amine, K., *Journal of the Electrochemical Society* 153(2):A316–A320, 2006.

[9] Kang, S.H., Sun, Y.K., and Amine, K., *Electrochemical and Solid State Letters* 6(9):A183–A186, 2003.

[10] Kang, S.H., and Amine, K., *Journal of Power Sources* 146:654–657, 2005.

[11] Amine, K., Belharoauk, I., Liu, J., Tan, T., Yumoto, H., and Ota, N., Abstract No: 2F09, 48th Battery Symposium in Japan. **Not enough info?**

[12] Nelson, P., Dees, D., Amine, K., and Henriksen, G., *J. Power Sources* 110(2):349, 2002.

[13] Nelson, P., Bloom, I., Amine, K., and Henriksen, G., *J. Power Sources* 110(2):437, 2002.

[14] Nelson, P., Liu, J., Amine, K., and Henriksen, G., *ECS Proc. Vol. (F1) Power Sources Modeling*, 2003.

[15] Argonne National Laboratory, PSAT (Powertrain Systems Analysis Toolkit), http://www.transportation.anl.gov/.

[16] Rousseau, A., Sharer, P., and Besnier, F., "Feasibility of Reusable Vehicle Modeling: Application to Hybrid Vehicles," SAE paper 2004-01-1618, SAE World Congress, Detroit, http://www.eere.energy.gov/vehiclesandfuels, March 2004.

[17] http://www.gm-volt.com/. **Need more info.**

[18] Karbowski, D., Rousseau, A., Pagerit, S., and Sharer, P, "Plug-in Vehicle Control Strategy: From Global Optimization to Real Time Application," 22nd International Electric Vehicle Symposium (EVS22), Yokohama, October 2006.

8. Authors

Paul Nelson, Chemical Engineer, Argonne National Laboratory, 9700 South Cass Avenue, Argonne, IL 60439-4815, USA

Paul Nelson is experienced in battery development and modeling. He received his Ph.D in Chemical Engineering from Northwestern University in 1958 and an MBA degree from the University of Chicago in 1977.

Khalil Amine, Senior Scientist, Argonne National Laboratory, 9700 South Cass Avenue, Argonne, IL 60439-4815, USA

Dr. Amine is a senior scientist who has been manager of the advanced battery program at Argonne National Laboratory since 1998. He manages and directs the development of advanced chemistries and battery systems at Argonne for HEV and PHEV applications. He obtained his Ph.D in Material Sciences at CNRS Laboratory, Bordeaux University, in 1989.

Hiroyuki Yumoto, Director of Cell Development, leads EnerDel's lithium ion cell activities. Mr. Yumoto has both a Bachelor’s degree in Industrial Chemistry and a Masters degree in Polymer Chemistry from Kyoto University. He has a Master’s degree in Material Science from the University of Southern California.

Aymeric Rousseau, Research Engineer, Argonne National Laboratory, 9700 South Cass Avenue, Argonne, IL 60439-4815, USA, arousseau@anl.gov

Aymeric Rousseau is head of the Advanced Powertrain Vehicles Modeling Department at Argonne National Laboratory. He received his engineering diploma at the Industrial System Engineering School in La Rochelle, France, in 1997.